Radiation Physics and Chemistry 216 (2024) 111365

Contents lists available at ScienceDirect

Radiation Physics and Chemistry

journal homepage: www.elsevier.com/locate/radphyschem

To what extent do field conditions affect gamma dose rate determination using portable gamma spectrometry?

Loic Martin [a,*], Mathieu Duval [b,c,e], Lee J. Arnold [d]

[a] Newton International Fellow, SUERC, Glasgow, UK
[b] National Research Centre on Human Evolution (CENIEH), Burgos, Spain
[c] Australian Research Centre for Human Evolution (ARCHE), Griffith University, Brisbane, Australia
[d] Environment Institute, And Institute for Photonics and Advanced Sensing (IPAS), School of Physics, Chemistry and Earth Sciences, University of Adelaide, Adelaide, Australia
[e] Palaeoscience Labs, Dept. Archaeology and History, La Trobe University, Melbourne Campus, Bundoora, 3086, Victoria, Australia

ARTICLE INFO

Handling Editor: Piotr Ulanski

ABSTRACT

Field gamma spectrometry is a widely used approach for determining *in situ* gamma dose rates in dosimetric (i.e., electron spin resonance and luminescence) dating applications. In comparison with laboratory-based determinations, *in situ* radioactivity measurements typically provide more representative gamma dose rate evaluations for heterogeneous sedimentary environments. However, it is often not possible to perform *in situ* gamma spectrometry measurements under carefully controlled conditions that are directly comparable to those originally used for equipment calibration.

In this study, we use Geant4 Monte Carlo simulations to model gamma spectrometry measurements under a range of field conditions, and examine the relative impacts of the following parameters on dose rate determination using the threshold calibration approach: (i) geometry and depth of the measurement hole in which the probe is inserted, (ii) nature of the sediment or rock materials and their water content, (iii) geometry of the radiation environment surrounding the measurement hole, i.e. closed and partially closed sites (e.g., caves, trenches) versus open-air sites (e.g. plain field excavations, cliff or cutting exposures).

Our results show that some differences in calibration and field measurement configurations can significantly bias *in situ* gamma dose rate determinations. Variations in the depth of probe holes can result in underestimations of infinite matrix gamma dose rates by 5% for a 30 cm-deep hole to 58% for measurements made against sediment surfaces (i.e., 2π geometry). Use of hole shapes that do not match those of the probe can lead to underestimations of infinite matrix dose rates by up to 4%, with these biasing effects becoming more significant for shallow holes. External gamma radiation originating from, and backscattered against, structures in the surrounding environment can contribute significantly to gamma dose rates measured using shallow probe holes. The nature of the mineral materials can have a small effect on the measured gamma dose rate (equivalent to infinite matrix dose rate biases of a few percent), mostly due to differences in the density of different materials. Measurements performed in materials with high water contents can be affected by small gamma dose rate overestimations due to differences between water attenuation factors of centimetre-scale objects such as gamma spectrometer probes and those of relevance for dating smaller objects such as sediment grains. These problems can be resolved by using specific correction factors, by including additional uncertainties during dose rate determination, or by performing *in situ* measurements at different depths for the same location.

1. Introduction

Dosimetric dating techniques, including optically stimulated luminescence (OSL), thermoluminescence (TL) and electron spin resonance (ESR), require environmental dose rate measurements for the dosimeter being dated, which is usually buried in sediment (e.g., Aitken, 1985). The gamma dose rate ($\gamma\,\dot{D}$), which typically accounts for about 30 % of the total dose rate, is commonly measured in the field as close as possible

* Corresponding author.
E-mail address: loic.martin@glasgow.ac.uk (L. Martin).

https://doi.org/10.1016/j.radphyschem.2023.111365
Received 31 January 2023; Received in revised form 9 August 2023; Accepted 24 October 2023
Available online 6 November 2023

to the original sample location in order to capture both short- and long-range gamma radiations, and any potential heterogeneities nearby. One of the most widely employed techniques for this purpose is portable γ spectrometry, which makes use of a scintillator probe coupled to a photomultiplier tube (Lovborg and Kirkegaard, 1974; Løvborg et al., 1979; Mercier and Falguères, 2007; Guérin and Mercier, 2011a; Guérin and Mercier, 2011b; Arnold et al., 2012). In order to accurately determine *in situ* γ Ḋ, it is necessary to carefully calibrate the detector (typically a NaI:Tl or $LaBr_3$:Ce crystal) under conditions that are comparable to those encountered at sites of interest. The threshold calibration method is commonly used for γ Ḋ determination using portable γ spectrometry, which is based on the principle that the count rate, or the rate of energy deposition, measured by the spectrometer above a certain energy threshold is directly proportional to the sediment dose rate at the point of measurement (Lovborg and Kirkegaard, 1974; Murray et al., 1978; Mercier and Falguères, 2007; Guérin and Mercier, 2011a; Duval and Arnold, 2013). The γ counts rate or γ energy deposition rate measured above the threshold value is converted into γ Ḋ by performing comparable γ spectrometry measurements on reference materials of known γ Ḋ. This method of calibration allows determination of γ Ḋ from on-site gamma spectrometry measurements performed over relatively short acquisition times (e.g. less than half an hour), making it convenient for field investigation.

In practice, however, field measurement conditions vary from site to site, and they often differ from the exact conditions of calibration. Sediment compaction, hardness and heterogeneity, for instance, can preclude drilling optimal holes that have exactly the same diameter as the probe, or that have the required depth to meet infinite matrix (Aitken, 1985) requirements. Moreover, the geometry of the surrounding radioactive environment may differ significantly between sites, with measurements performed variously in open-air settings (such as flat areas, beaches without nearby relief, hill tops) and (semi-) enclosed settings (such as caves or narrow trenches). The extent to which these variable field conditions impact the accuracy of *in situ* γ Ḋ measurements remains somewhat unknown because of the difficulty of carrying out γ Ḋ experiments under a range of controlled conditions. Consequently, methods used for mitigating against these complications remain approximations and the potential exists for possible biases in field γ Ḋ determinations.

Monte Carlo modelling is increasingly being used to simulate dose rates for routine luminescence and ESR dating applications (e.g., Fain et al., 1999; Guérin and Mercier, 2012; Martin et al., 2015b; Duval and Martin, 2019). This approach offers the advantage of providing accurate Ḋ calculations where *in situ* measurements are not possible, or where they are difficult to perform. Modelling of complex dosimetric environments, such as heterogeneous sediments and rocks for which many parameters need to be taken into account, remains challenging. However, it is often possible to create idealised representations and to vary one model parameter at a time in order to systematically investigate individual effects on the final Ḋ output. Such modelling exercises are conceptually similar to field or laboratory experimental setups in which ideal sedimentary configurations are physically reconstructed, and parameters of interest are strictly controlled in order to assess their individual effect on Ḋ evaluation. For example, such experiments have been successfully used previously to assess the reliability of Monte Carlo modelling for β Ḋ evaluation (Nathan et al., 2003).

Here we use Monte Carlo modelling with Geant4 (Agostinelli et al., 2003) in order to investigate and quantify the potential impacts of different environmental parameters on field γ spectrometry measurements. The accuracy of the Geant4 modelling framework for representing complex geometries and various media, as well as transport and interaction of low energy particles and secondary emissions, has been demonstrated previously (Agostinelli et al., 2003; Guérin and Mercier, 2012; Martin et al., 2015c). These prior Geant4 studies provide the necessary foundation for reliable modelling of different measurement condition commonly encountered in portable γ spectrometry applications and for precise determination of counts and energy deposited within probe scintillator crystals. After modelling the effects of performing γ Ḋ determinations by threshold method under a range of simulated field measurement configurations, we go on to propose a series of practical solutions for mitigating against the most significant biasing effects.

2. Modelling conditions

The Geant4 toolkit for Monte Carlo simulations of particle-to-matter interactions was used to write code for simulating *in situ* determination of γ spectrum using a gamma spectrometer with a scintillation detector, and for determining the corresponding γ Ḋ using the threshold calibration method. This code, named MIGAS (Modelling In-situ Gamma Spectrometry), includes options for modifying a series of input parameters to simulate different field conditions and measurement configurations, such as: (i) the nature of the mineral material (i.e., chemical composition and average density), water content and size of the mineral block, (ii) the geometry and composition of the scintillator probe, and (iii) the size and shape of the probe measurement hole in the mineral block. The code also includes an option for adding a wall or structural feature in front of the measurement area in order to simulate external γ contributions and backscattering γ particles from nearby objects (see Fig. 1 and Fig. 2 for geometries). The MIGAS code uses Geant4 version 10.03, together with the Geant4 library PENELOPE code for low energy particle physics (Baró et al., 1995; Ivanchenko et al., 2011).

As a baseline configuration, we created a 175 × 175 × 175 cm cubic mineral block composed of SiO_2 with a density of 1.8 g cm^{-3}, which corresponds to a typical sediment deposit with an average atomic mass (Z). The measurement hole for the spectrometer probe is placed at the center of the block's front face and oriented longitudinally along the Z axis of the block, ensuring at least 80 cm of sediment between the probe and the side/back edges of the block (Fig. 1). Unless otherwise stated, the diameter of the hole is the same as the diameter of the probe, which represents an ideal measurement scenario. A particle reflection algorithm was implemented to redirect leaving particles towards the simulated volume at reflection angles (Fig. 1). This is similar to the function used by Guérin and Mercier (2012) and Martin et al. (2015c), and is meant to reproduce an irradiation field of infinite extent in the X and Y planes. The latter is especially required when modelling surface (2π) measurement cases or when dealing with an external γ Ḋ component.

The probe was modelled using the dimensions and composition of a two-inch NaI probe supplied with a Canberra Inspector 1000 gamma spectrometer, which is widely used in the luminescence and ESR dating community (e.g., Arnold et al., 2012; Duval and Arnold, 2013). Consequently, we specified a 7.5 cm-long cylinder with a diameter of 6.5 cm, including protective outer layers of rubber and aluminium shielding with thicknesses of 6 mm and 1 mm, respectively (Fig. 2). The scintillator crystal of the probe is composed of a 6.7 cm-long and 5.1 cm-diameter NaI cylinder with a density of 3.67 g cm^{-3}. The Tl doping has virtually no impact on the overlap density of the crystal and was therefore not considered in the simulations. Preliminary tests carried out with and without the simulation of a 25 cm-long and 4 cm-diameter filled aluminium handle showed negligible differences in the resulting γ Ḋ determinations (<0.1%). Therefore, subsequent simulations were carried out without the handle.

MIGAS was used to test the effect of changing various measurement parameters that potentially act as sources of uncertainty for γ Ḋ measurements in routine dating studies, namely: (i) the depth of the measurement hole in the sediment block, (ii) the shape of the measurement hole, (iii) the material (mineral composition and density) of the block, (iv) the water content of the block, and (v) the geometry and radioactivity of the surrounding environment. The measurement configurations tested for each of these modelling experiments is detailed in the following sections.

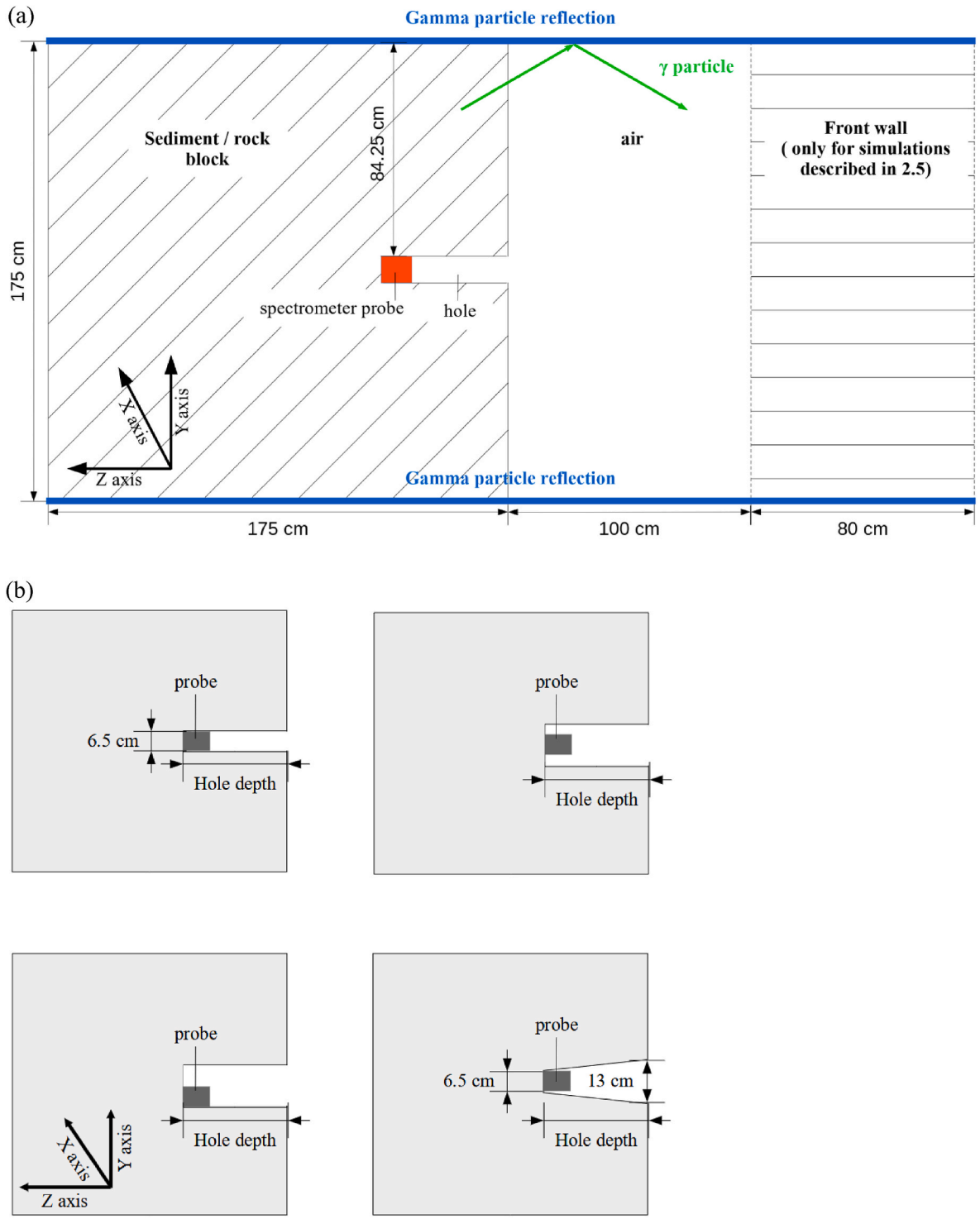

Fig. 1. Geometry of the simulated environment. (a) Main geometry. (b) Geometry of the probe measurement holes. *The different hole geometries simulated are: (i) hole with diameter equivalent to that of the spectrometer probe (*6.5 cm*), (ii) hole with twice the diameter of the probe, and probe sitting in the middle of the hole, (iii) hole with twice the diameter of the probe, and probe lying on one side of the hole, (iv) conical hole with an outer-end diameter of* 13 cm*, and an inner-end diameter equivalent to that of the probe (*6.5 cm*).*

2.1. Depth of the measurement hole

Field γ spectrometry measurements are often carried out by placing the probe in a 30 cm-deep hole, in order to closely meet infinite matrix conditions (γ Ḋ >95% of the infinite matrix γ Ḋ according to Aitken, 1985). However, creating cylindrical holes that reach 30 cm depths is sometimes difficult, and may not always be possible due to the nature and compaction of the sediment. This is particularly true where the sediment is loose or prone to collapse, contains abundant clasts or blocks, or is highly cemented and very hard to drill. In such circumstances, the only practical option might be to undertake γ Ḋ measurements in holes that are less than 30 cm deep. To examine the effects of making *in situ* γ Ḋ measurements using optimal and sub-optimal depths, we carried out a series of simulations in which the depth of the probe

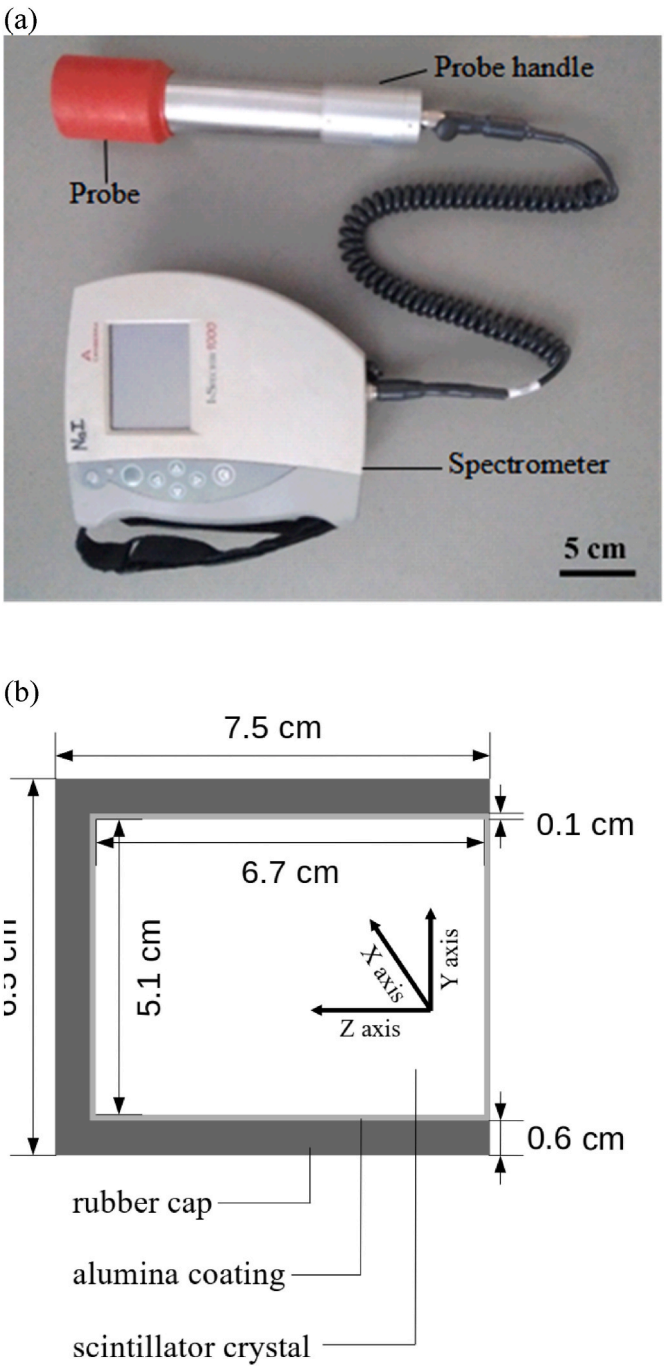

Fig. 2. The γ spectrometer probe. (a) Canberra Inspector 1000 gamma spectrometer with 2 × 2 inch NaI probe. (b) Configuration of the simulated NaI probe used in the modelling experiments.

hole was varied from 80 cm to 0 cm. These end-member probe depths closely approximate 4π and 2π measurement geometries, respectively.

2.2. Shape of the measurement hole

Ideally, the dimensions of the hole used for *in situ* γ Ḋ evaluation should be as close as possible to the dimensions of the probe itself (i.e., cylindrical and of the same diameter), in order to minimise the influence of void space on the resultant measurement. However, practical limitations at sampling sites may result in measurement holes being significantly wider than the probe, either at both ends of the hole (retaining the overall cylindrical shape of the hole) or just at the outer end of the hole (resulting in a more pronounced conical shape). Such hole configurations result in smaller solid angles of irradiation in comparison to measurements made using ideal hole geometries (i.e., holes with the same diameter as the probe), which can potentially have non-negligible effects on γ Ḋ measurements. To examine these effects further, we simulated an extreme scenario of γ Ḋ evaluation where the hole was twice as wide as the diameter of the probe, and the probe was either positioned at the center of the hole or lying on one side of the hole. We also repeated the simulation using a conical-shaped hole that had an outer-end diameter twice as wide as the probe, and an inner-end diameter equivalent to that of the probe (see Fig. 1b).

2.3. Composition of the sediment block

The density and mineral composition of sediments and rocks vary significantly in nature, and this can affect the propagation ranges of γ radiations across different dating sites. We have therefore modelled γ particles in the context of field γ spectrometry measurements across a range of materials, each characterized by different chemical compositions and density, as summarized in Table 1.

2.4. Sediment water content

Natural sediment deposits can contain significant quantities of pore water, particularly in closed environments such as caves, or in humid open-air settings (e.g. tropical or coastal sites). In contrast, the calibration of γ spectrometer probes is usually performed under drier conditions using low porosity reference blocks. While the attenuating effect of water content on Ḋ evaluation is routinely considered in dosimetric dating studies, the magnitude of this effect may differ for the γ spectrometer probe when compared with the (usually smaller) object being dated (e.g., quartz grains or fossil teeth). Zimmerman (1971) determined a γ Ḋ water attenuation factor (χ) of 1.14 for sedimentary grains, where χ is expressed as the ratio of effective mass stopping powers of γ rays between water and alumina, and with the stopping power of alumina being assumed to be close to that of sediment. The suitability of this value was later confirmed by Aitken and Xie (1990) and Guérin and Mercier (2012) using different approaches (integration of the gamma absorption equation over the effective gamma spectra, and Monte Carlo simulations with Geant4, respectively), whereas Nathan and Mauz (2008) calculated a lower value of 1.02 using Monte Carlo N-Particle (MCNP) simulations. Aitken and Xie (1990) also obtained different χ values of 1.14 and 1.065 for small objects <1 mm size (e.g., sedimentary grains) and dry objects >1 cm (e.g., γ spectrometer probes), respectively. These differences reflect the fact that most of the γ radiation energy is deposited through secondary β emissions. These β emissions are partially absorbed by water in the sediment pore spaces before reaching small objects, whereas they are not affected by any water attenuation inside large dry objects (Aitken, 1985).

In order to determine a more suitable χ value for *in situ* γ

Table 1
Composition of the different sedimentary environments used in the simulations.

Name	Density (g. cm^{-3})	Chemical composition (% in mass)
Soil[a]	1.6	O 50.0%, Si 36.0%, Al 6.9%, Fe 3.5%, K 1.5%, Na 0.6%, Ti 0.6%, Ca 0.5%, Mg 0.4%
organic-rich soil[b]	1.6	O 38.3%, C 29.0%, Ca 9.7%, Si 5.4%, Cl 4.1%, P 3.3%, Mg 2.2%, K 1.9%, Na 1.9%, N 1.2%, Al 1.0%, Fe 0.7%, S 0.7%, F 0.5%, Ti 0.1%
Quartz sand	1.8	O 52.6%, Si 47.4%
Clay	1.8	O 46.5%, Si 20.4%, Al 19.6%, Fe 13.5%
Concrete	2.3	O 47.8%, Si 26.6%, Al 11.3%, Fe 8.2%, Ca 6.1%
Carbonate	2.6	O 47.9%, Ca 40.0%, C 12.1%,
Granite	2.7	O 48.2%, Si 31.5%, Al 11.4%, K 5.6%, Na 3.3%,

[a] From Aitken (1985), appendix H, table H.1.
[b] From Guérin and Mercier (2011a).

spectrometry measurements, we simulated the effect of water content on γ Ḋ determination in different sedimentary environments (from Table 1) by varying water content from 0% to 100% of dry mass. χ values were calculated from the γ spectrometry simulation results and compared with published χ values for γ Ḋ determination.

2.5. Surrounding environment and backscattered γ contributions

When performing routine measurements in sediment deposits or rocks, it is possible for the probe count rate to be influenced by γ rays originating from outside the sediment deposit itself; particularly if the probe measurement hole is not deep enough to meet infinite matrix conditions (<30 cm). In the case of non-invasive surface (2π) γ spectrometry measurements, which would theoretically correspond to about 50% of the infinite matrix γ Ḋ value, it can be especially difficult to separate the γ Ḋ contributions originating from the analyzed material and those originating from external sources in the surrounding environment (Guérin and Mercier, 2011b). In addition, previous modelling experiments (Martin et al., 2015c) have shown that backscattering of γ rays from nearby structures (e.g., cave walls, adjacent sediment sections, nearby rocks) can have a significant influence on γ Ḋ determination at the surface or at shallow depths beneath the surface of the sediment or rock.

In order to investigate the potential effects of external and backscattered γ ray contributions on portable γ Ḋ measurements, we performed a series of simulations that included a wall in front of the material block and measurement hole. For each simulation, we varied the probe hole depth from 0 cm (2π measurement) to 80 cm (infinite matrix conditions). γ Ḋ contributions from the main block and from the adjacent wall were simulated separately in order to differentiate between γ Ḋ contributions originating directly from the nearby structure and γ Ḋ contributions from backscattered γ rays originating from the main sediment block itself. These contributions were then combined to derive more realistic γ Ḋ scenarios.

2.6. Simulation of a portable gamma spectrometer

The γ emission spectrum of energies (i.e. the energy spectra of primary γ particles generated during the Geant4 simulation) used for the portable γ spectrometer simulations have been derived by mixing ^{40}K, U-series and Th-series γ ray energy spectra from natural radioactive decay (assuming the series are in secular equilibrium) in proportions equivalent to sediment elemental concentrations of 1% K, 3 ppm U and 10 ppm Th (Aitken, 1985) (Fig. 3). These spectra were obtained with the Geant4 radioactive decay process (Hauf et al., 2013), and are based on the evaluated nuclear data files (ENSDF) datasets (from the ENSDF database on October 25, 2013. Version available at http://www.nndc.bnl.gov/ensarchivals/). The Geant4 Monte Carlo simulations involve creating an initial particle and then following the particle interaction in the media step-by-step. In MIGAS, the primary γ particles (referred as γ emissions) are generated one-by-one with an initial energy randomly selected from the known energies of the γ spectrum and according to their emission probabilities. The point of origin of these γ emissions are specified as either within the simulated material block or within the front wall, depending on the simulation. Each γ particles is subsequently simulated step-by-step, and eventually interacts with the NaI crystal of the spectrometer and deposits a certain energy. The spectra of energy deposited by each γ particle in the simulated NaI crystal were recorded for each modelling experiment from 0 keV to 4000 keV with a resolution of 1 keV. The number of counts or the energy deposited above a threshold of 300 keV were summed in order to simulate, respectively, a count threshold calibration (Lovborg and Kirkegaard, 1974; Mercier and Falguères, 2007) and an energy threshold calibration (Guérin and Mercier, 2011a) of the spectrometer. We observed a directly proportional relationship between the simulated calibrations and the simulated dose rate, as reported by Guérin and Mercier (2011a). No significant difference was observed between the results obtained using the energy threshold and the count threshold methods, in agreement with the findings of Guérin and Mercier (2011a). As such, we adopt the generic term 'threshold calibration' to describe the results obtained from the modelling simulations. It is also possible to simulate the number of counts in specific energy windows corresponding to ^{40}K, ^{238}U-series or ^{232}Th-series photoelectric peaks using our simulated datasets. However, we have not evaluated the 'energy windows' approach of γ Ḋ evaluation in this study because the lower probability of events occurring in these specific photoelectric peak energy windows would require much longer simulation times to obtain sufficient statistical precision.

The probability of γ interactions in the crystal, as well as edge effects due to secondary γ rays and β particles leaving the crystal, were taken into account by the Monte Carlo simulations. We assumed a linear and homogeneous relationship between the energy deposited in the crystal by one primary photon and the signal measured in the scintillation volume, which implies proportionality between pulse intensity and measured signal. However, we acknowledge that this proportionality assumption may not strictly hold due to variability in scintillation efficiency with the energy of interaction, and variability in photon transmission from the interaction point in the crystal to the photo-multiplier tube (Saito and Moriuchi, 1981). Unfortunately, evaluating the effects of

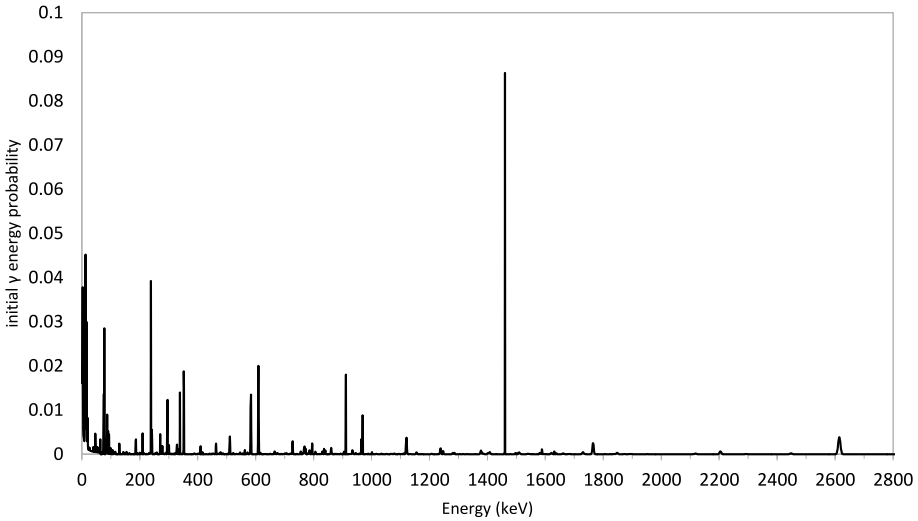

Fig. 3. Example energy spectrum of gamma emissions used in the simulations.

such variation is beyond the scope of the present study, as it would require complex modelling of the scintillator, and would detract from our main focus of evaluating the influence of external parameters on *in situ* γ Ḋ determination.

This spectrum shows the probability of a γ emission (i.e a γ particle generated in the simulation) on the Y axis as a function of its initial energy. It corresponds to a sediment or rock material with elemental concentrations as follows: 1% K, 3 ppm U, and 10 ppm Th. The full spectrum used for the simulations includes all known X-ray and γ emissions from 0 keV to 4000 keV.

3. Results

Each modelling configuration outlined in Sections 2.1–2.5 was simulated five times with 10^9 γ particles simulated for each run. Each individual run took about 24 h to complete on a standard desktop computer. The uncertainties on the average results from each experiment were calculated using the standard deviation of values obtained for the five repeated runs and correspond to the 95% confidence intervals of the Student's t-distribution. For all simulations, the uncertainty on the full γ Ḋ deposited in the probe is less than 1%, while the uncertainty on the γ Ḋ calculated using the threshold approach is less than 2%.

All modelled γ Ḋ results have been normalised to the results obtained from simulations in an 80 cm-deep hole that has the same diameter as the probe (6.5 cm). For this baseline modelling configuration, the probe receives a γ Ḋ equivalent to >99% the infinite matrix γ Ḋ; it is therefore considered a suitable approximation of simulations or measurements made in infinite matrix geometry, or 4π geometry.

3.1. Depth of the measurement hole

Fig. 4 shows how the normalised γ Ḋ (γ Ḋ from the simulated measurement as a percentage of the results in infinite matrix conditions) varies with depth of the probe measurement hole. The γ Ḋ obtained for a 30 cm-deep probe hole represents ~95% of the baseline configuration γ Ḋ obtained by simulating an 80 cm-deep probe hole, which is the closest approximation to full 4π geometry (= infinite matrix conditions). This relationship is consistent with the previous calculations of Aitken (1985). The normalised γ Ḋ decreases considerably for measurement holes that are shallower than 25 cm and may result in significant bias in γ Ḋ determination if the limited probe hole depths are not taken into account.

It is noteworthy that the γ Ḋ from simulated measurements in 2π geometry (i.e., the scenario whereby the probe is placed against the outer surface of the sediment block; measurement depth = 0 cm) corresponds to < 50% of the baseline configuration γ Ḋ measured at 80 cm depth (as well as the γ Ḋ measured at 30 cm depth). This is due to a deficit of backscattered γ particles at the interface between the sediment or rock material and air: γ particles randomly change direction after a Compton interaction, and if this happens near the surface of the block there is a non-negligible possibility that some γ particles escape the block. In this scenario, there is a very low probability of interaction with the air which could send backscattered particles toward the block, creating a γ Ḋ deficit at the surface of the sediment. This finding is consistent with the results of Martin et al. (2015c) and will be further discussed in Section 3.5.

Fig. 5 shows that small reductions in normalised γ Ḋ occur at a given measurement depth when using holes twice the diameter of the probe or when using holes that have different shapes to the probe. The γ Ḋ from simulated measurement, expressed as a percentage of the Ḋ simulated in infinite matrix conditions, differ by 2–4% in comparison to modelling scenarios where the measurement hole diameter and shape is equivalent to the probe (black circles in Fig. 5), with slightly larger normalised γ Ḋ offsets obtained for shallower holes. The differences in normalised γ Ḋ may be considered relatively minor for 30 cm-deep probe holes (representing 92%–94% of the infinite matrix γ Dr). However, when combined with hole depths effects, the offsets become significant for shallower holes (e.g., 58–59% of the infinite matrix γ Ḋ for a depth of 7.5 cm).

Interestingly, there is very little difference in normalised γ Ḋ (<2%) at a given depth for the three different hole shape configurations considered (i.e., 13 cm diameter hole with probe sitting at the center; 13 cm diameter hole with probe aligned with one side; conical shaped hole with an outer-end diameter of 13 cm and an inner-end diameter

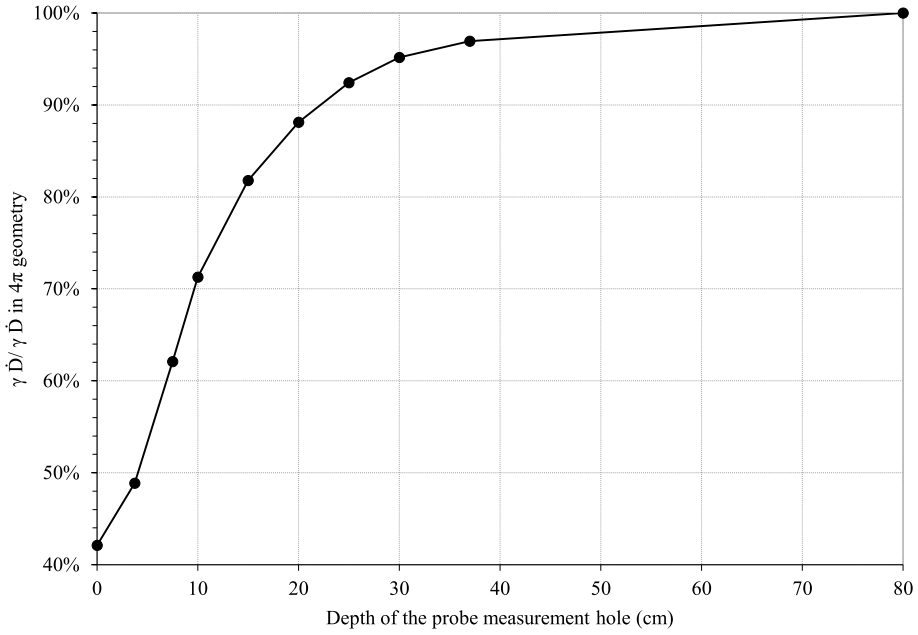

Fig. 4. Relationship between the normalised γ Ḋ and the depth of the probe measurement hole. *To derive these data, a baseline threshold calibration configuration was first simulated in which the measurement hole was* 80 cm-*deep and had a diameter equivalent to that of the probe (4π geometry). The γ Ḋ obtained by undertaking simulations using different hole depths is expressed as a percent of the baseline configuration γ Ḋ, which corresponds to the result of the simulated measurement in infinite matrix geometry (4π). The numerical data used to derive this plot can be found in the Supplementary Material SD1.*

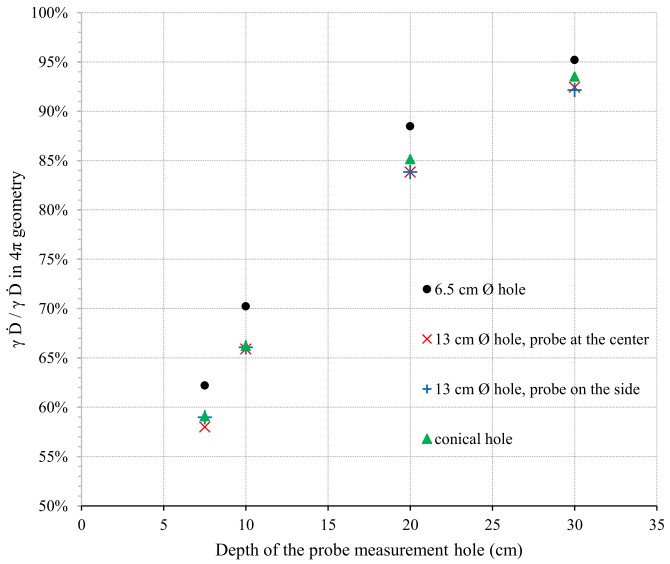

Fig. 5. Relationship between the normalised γ Ḋ from simulated measurements and the shape of the probe hole for simulations undertaken using different hole depths. The geometries of the probe holes are illustrated in Fig. 1b.
To derive these data, a baseline threshold calibration configuration was first simulated in which the measurement hole was 80 cm*-deep and had a diameter equivalent to that of the probe (4π geometry). The γ Ḋ obtained by undertaking simulations using different hole shapes and depths is expressed as a percent of the baseline configuration γ Ḋ, which corresponds to the result of the simulated measurement in infinite matrix geometry (4π). The numerical data used to derive this plot can be found in the Supplementary Material SD2.*

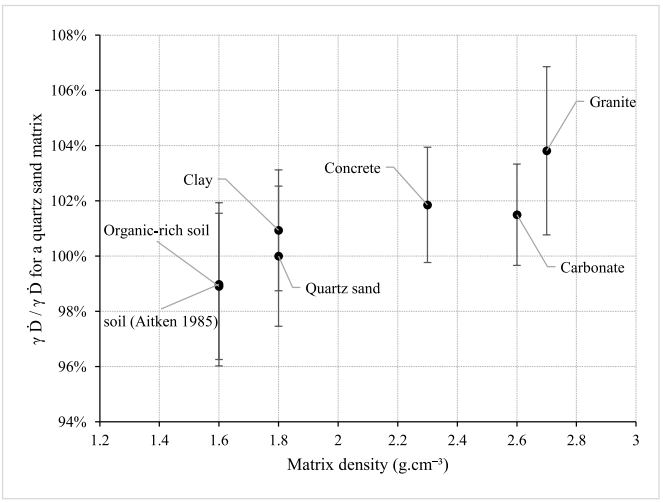

Fig. 6. Relationship between normalised γ Ḋ from simulated measurements and density of the block material. *To derive these data, a baseline threshold calibration configuration was first simulated for a quartz sand material (SiO_2, density* 1.8 g cm^{-3}*) using a measurement hole that was* 30 cm*-deep and had a diameter equivalent to that of the probe. The γ Ḋ obtained by undertaking simulated measurements in different materials are expressed as a percent of the baseline configuration γ Ḋ obtained for the quartz sand material. For all materials considered, the measurement hole was* 30 cm*-deep and had a diameter equivalent to that of the probe. The chemical composition and density of the different materials are given in Table 1. The numerical data used to derive this plot can be found in the Supplementary Material SD3.*

equivalent to that of the probe). This suggests that the exact shape of the hole has limited influence on the measured γ Ḋ once the diameter of the hole is larger than that of the probe (i.e., >6.5 cm diameter). Additional simulations using a broader range of hole shapes and diameters would nevertheless be needed to confirm this observation.

3.2. Composition of the sediment block

Fig. 6 shows that the composition and density of the block material can influence the γ Ḋ by up to several % compared to the baseline simulation performed using a quartz sand matrix and a 30 cm-deep measurement hole. There is an apparent correlation between simulated γ Ḋ and material density, which most likely reflects differences in the average range of γ particles for different densities. In other words, γ Ḋ measurements made using a 30 cm-deep probe hole will more closely approximate true 4π geometry (= infinite matrix conditions) for high-density materials compared to lower density materials, simply because the average range of γ rays is shorter for the former case. However, the dependency of normalised γ Ḋ on material density and composition seems limited (<5 % differences compared to baseline simulations with quartz sand matrix) and the size of the associated uncertainties preclude further interpretation of the simulated data set.

3.3. Sediment water content

The modelled γ Ḋ water attenuation factors (χ) obtained by varying water from 0% to 100% dry mass for different simulated sediment materials are summarized in Fig. 7, and compared with χ values published previously (Zimmerman, 1971; Aitken and Xie, 1990; Nathan and Mauz, 2008; Guérin and Mercier, 2012). The χ values from our simulations are similar to the values published by Aitken and Xie (1990) and Guérin and Mercier (2012) for centimetric-scale objects such as γ spectrometer probes, though they are systematically lower by 1–6%. The reason for this minor difference may be that we have simulated γ spectrometry measurements performed in 30 cm-deep probe holes whereas these previous studies considered 4π geometry, and therefore part of the high-energy γ ray contribution is missing. The average γ Ḋ χ value from our simulations for different sedimentary materials is 1.02 ± 0.03, where the uncertainty represents the maximum deviation observed between χ values for different materials and the average χ value.

Fig. 7 also shows that there are significant differences between the χ values simulated for the spectrometer probe and those published previously for smaller (sub-millimetre) objects such as sediment grains (e.g., Zimmerman, 1971). It is noteworthy that Nathan and Mauz (2008) calculated a γ Ḋ χ value of 1.02 ± 0.04 for sedimentary grains, which is significantly lower than all other published χ values for sediment grains but comparable to the values published for larger objects (Aitken and Xie, 1990; Guérin and Mercier, 2012). The authors attributed this difference to small variations in the γ spectra used in their simulations. However, this explanation is not supported by the agreement observed between the χ values calculated by Zimmerman (1971), Aitken and Xie (1990) and Guérin and Mercier (2012), all using different models and updated spectra. Another possibility is that the MCNP5 particle transport code used by Nathan and Mauz (2008) was not adapted to low-energy, secondary β particle physics, as examined by Koivunoro et al. (2012). We consider this explanation more likely, considering that the differences observed between water attenuation by sediment grains and larger objects is attributable to secondary β particle interactions (Aitken and Xie, 1990).

The difference between the χ values from simulation of the spectrometer probe (average = 1.02 ± 0.03) and those published previously for sediment grains (typically 1.14 for sediment grains, 1.07 for centimetre size objects) implies that the γ Ḋ measured using *in situ* γ spectrometry for wet sediment matrices is not directly equivalent to the γ Ḋ absorbed by the sediment grains targeted for dating. The difference between the γ Ḋ calculated using an χ value suitable for sediment grains and an χ value suitable for scintillator probes is displayed on Fig. 8 for sediment water contents ranging from 0% to 30% of the dry sediment mass. Apparent overestimations of the γ Ḋ from field γ spectrometry measurement on the order of <2% can be expected for sediments having

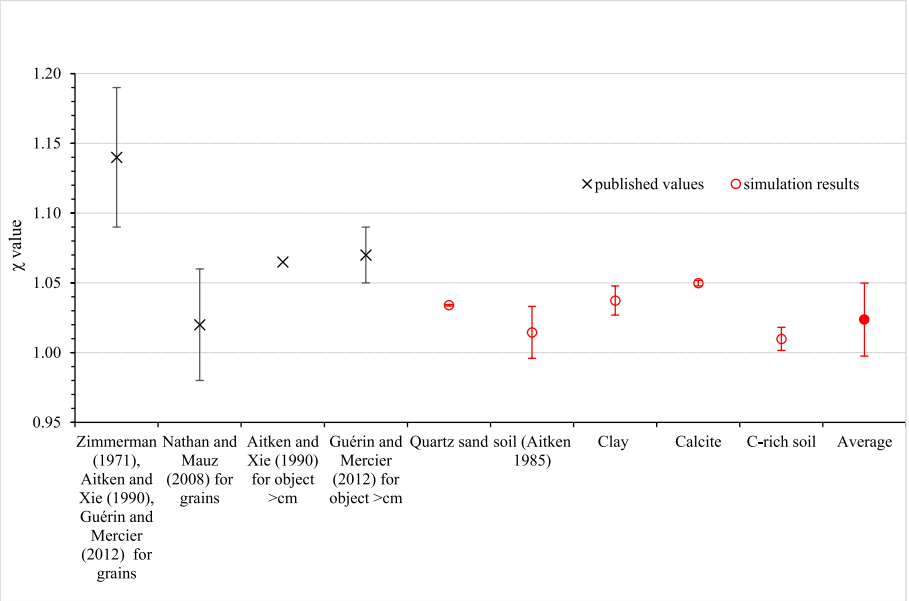

Fig. 7. γ Ḋ water attenuation factors (χ) published previously for sediment grains and larger (centimetre-sized) objects such as γ spectrometer probes, and χ values obtained in our simulated measurements by varying water from 0% to 100% dry mass for different sediment materials. *For all materials considered, the simulated measurement hole was* 30 cm-*deep and had a diameter equivalent to that of the probe. The numerical data used to derive this plot can be found in the Supplementary Material SD4. The uncertainty on the χ value for sediment grains reflects variability in grain size and radioelements considered (^{40}K, U-series or Th-series), as examined by Guérin and Mercier (2012).*

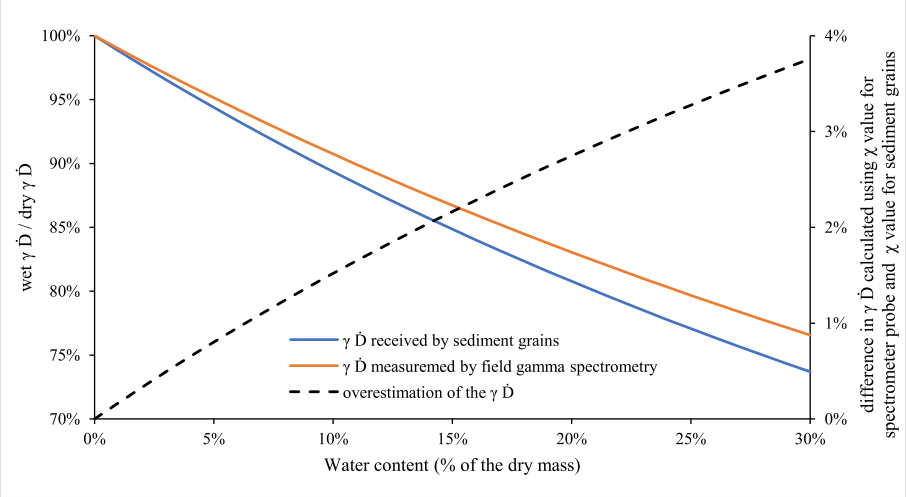

Fig. 8. Comparison of wet γ Ḋ for water contents in sediment ranging from 0% to 30%, using χ values derived for sediment grains and γ spectrometer probes according to Zimmerman's equation (1971). *The normalised γ Ḋ data are expressed as percent of the dry γ Ḋ. The solid blue line (read off the primary Y-axis) represents the γ Ḋ/dry γ Ḋ received by sediment grains calculated using an χ value of 1.14 for sediment grains (from Zimmerman, 1971, and confirmed by Aitken and Xie, 1990; Guérin and Mercier, 2012). The solid orange line (read off the primary Y-axis) represents the γ Ḋ/dry γ Ḋ that would be measured by field γ spectrometry using the χ value of 1.02 ± 0.03, as determined by our simulations. The difference in the γ Ḋ calculated using χ values for sediment grains and the probe (difference between the orange and blue curves) is shown as a dotted black line and is read off the secondary Y-axis. This dotted black line represents the theoretical systematic overestimation of the γ Ḋ from measurements by field γ spectrometry that could result from either using the in situ measurement as representative of the gamma dose rate for sediment grains over time (i.e., considering that the water content in the sediment at the time of measurement is representative of the water content over the time) or calculating a dry gamma dose rate by inaccurately correcting the γ spectrometry measurements using an χ value derived for sediment grains (1.14 ± 0.03) instead of an χ value that is suitable for the spectrometer probe (1.02 ± 0.03). The numerical data used to derive this plot can be found in the Supplementary Material SD5.*

water contents <10% owing to the fact that *in situ* γ spectrometry measurements are water attenuated at the time of acquisition according to an χ value for centimetre size object (1.02 ± 0.03) rather than an χ value that is relevant for the millimetre size sediment grains targeted for dating (1.14 ± 0.03). These apparent overestimations of probe γ Ḋ values increase to almost 4% for a sediment close to water saturation at 30%.

3.4. *External and backscattered γ Ḋ contributions*

Tests performed using varying distances between the main block (containing the probe hole) and the front wall (with distances ranging from 30 cm to 10 m) returned largely indistinguishable results. In effect, this means that a 10 m-thick layer of air does not significantly absorb γ rays compared to the block of material. The distance between the block

and the wall is therefore not considered a relevant parameter in this study. Consequently, the wall distance was arbitrary set to 1 m for all simulations considered here.

Fig. 9 compares normalised γ Ḋ (γ Ḋ from simulated measurements as a percentage of a simulated measurement in infinite matrix conditions - 4π) for different probe hole depths in two main configurations: (i) open field conditions, and (ii) closed site conditions with a wall placed in front of the block and measurement hole. The open field condition represents the standard geometry used for all simulations detailed in the previous sections, with no external wall structure in the direct vicinity of the simulated measurement point. The closed site conditions simulate measurements made in a radioactive block that is surrounded by, or facing, an inert structure, such as a limestone wall that has negligible radioactivity. This is a typical configuration for *in situ* gamma spectrometry measurements made in cave environments. The difference in normalised γ Ḋ profiles resulting from simulations of the two configurations using a range of measurement hole depths primarily reflects the degree to which the inert wall backscatters γ particles emitted within the block. Backscattered γ particles contributes negligibly to the normalised γ Ḋ (<1 %) for holes deeper than 10 cm (difference between red and blue lines on Fig. 9), as this hole depth corresponds to the average range of backscattered γ particles in sedimentary material. Interestingly, the normalised γ Ḋ obtained from the simulation of a 2π geometry probe measurement (0 cm probe hole depth) equates to 50% of the infinite matrix (4π geometry) γ Ḋ from simulated measurements when an inert wall is present. This is because backscattered γ particles from the inert wall compensates for the deficit of backscattered γ particles at the surface of the sediment block when simulating a measurement in 2π geometry. This mirroring effect in enclosed environments was previously described by Liritzis (1989), who noted similar backscattered γ Ḋ contributions: about 15% of the γ Ḋ measured at the sediment surface were attributable to backscattered γ rays in that study.

As part of the closed site configuration simulations, we also evaluated the effect of including an external wall that had the same radioactivity as the main block. This configuration is frequently encountered when *in situ* gamma spectrometry measurements are performed within a trench that is several meters deep and/or wide. Fig. 9 shows a marked decrease in relative γ Ḋ contributions from the radioactive wall (as a percentage of the γ Ḋ from simulated measurement in the sediment block) with increasing probe hole depth (green line; read off the secondary Y axis). However, non-negligible γ Ḋ contributions from the radioactive wall can still be observed for 30 cm probe hole depths (equating to ~4 % of the γ Dr from simulated measurement in infinite matrix conditions).

The true magnitude of external wall γ Ḋ contributions in cave or trench dating applications will depend on relative differences in the radioactivity of the measured sediment or rock and the front wall. In order to explore these influences further, we expanded our range of closed site simulations to include two additional configurations (in addition to the aforementioned configurations of having an inert front wall, and a front wall having the same radioactivity as the sediment block): namely, (i) a front wall having radioactivity equivalent to half that of the sediment block, (ii) front wall having radioactivity twice that of the sediment block. These configurations were simulated by applying a multiplication factor to the external wall γ Ḋ contribution dataset presented in Fig. 9 (with the multiplication factors varying from 0 for an inert wall to 2 for a wall with radioactivity twice that of the sediment block). The resultant wall γ Ḋ contributions were added to the γ Ḋ obtained for the radioactive block simulation when an inert wall is present and expressed as a percent of the γ Ḋ from simulation in infinite matrix conditions (4π geometry) for a range of different probe hole depths. The results obtained from these simulations are presented in Fig. 10.

Fig. 10 reveals that γ Ḋ contributions from a wall having radioactivity equivalent to the sediment block effectively act to recreate 4π measurement conditions for all probe hole depths, i.e., the normalised γ Ḋ equates to the infinite matrix t γ Ḋ for any depth of simulated measurement. This is because the air layer between the sediment block and the wall does not significantly absorb γ particles and because the wall and block sizes are virtually infinite with respect to particle reflection dynamics. Consequently, the combined wall and block γ Ḋ contributions equate to full 4π irradiation geometry. This type of scenario would correspond to *in situ* γ spectrometry measurements made in a trench of

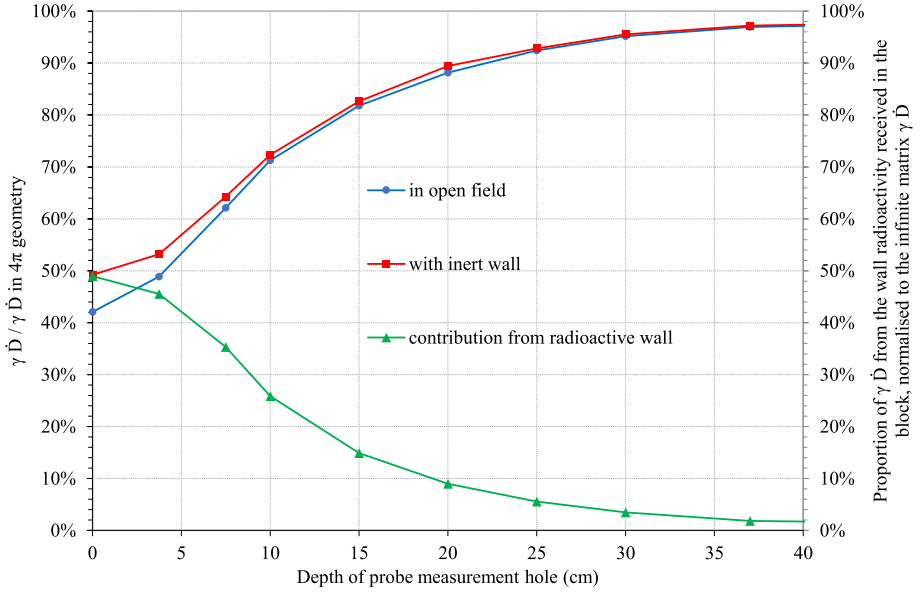

Fig. 9. Relationship between normalised γ Ḋ and depth of probe measurement hole for simulations that include no external wall, an inert external wall, and an external wall with radioactivity equivalent to the block. *To derive these data, a baseline threshold calibration configuration was first simulated in which the measurement hole was* 80 cm*-deep and had a diameter equivalent to that of the probe (4π geometry). The γ Ḋ obtained by undertaking simulations using different measurement hole depths and external wall configurations is expressed as a percent of the baseline configuration γ Ḋ. The normalised γ Ḋ obtained with no external wall (blue line) and an inert external wall (red line) are read off the primary Y axis (left). The γ Ḋ contributions from the radioactive wall (expressed as a percentage of the γ Ḋ from simulation in infinite matrix conditions in the block) are shown as a green line and read off the secondary Y axis (right). The numerical data used to derive this plot can be found in the Supplementary Material SD6.*

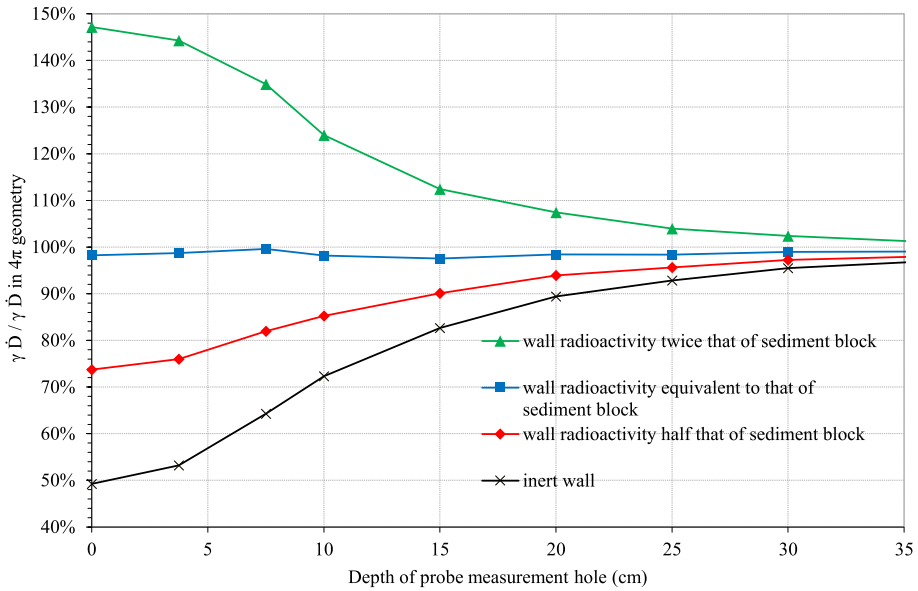

Fig. 10. Relationship between normalised γ Ḋ from simulated measurements and depth of measurement hole for simulations that include external walls with different radioactivity properties. *To derive these data, a baseline threshold calibration configuration was first simulated in which the measurement hole was* 80 cm-*deep and had a diameter equivalent to that of the probe (4π geometry). The γ Ḋ obtained by undertaking simulations using different measurement hole depths and external wall radioactivity configurations is expressed as a percent of the baseline configuration γ Ḋ from simulated measurement in infinite matrix conditions (4π geometry). The numerical data used to derive this plot can be found in the Supplementary Material SD7.*

homogeneous sediment, assuming that the proportion of γ rays exiting the trench are not significant.

Fig. 10 also shows that external γ Ḋ contributions originating from, and backscattered against, surrounding structures can have significant effects on field γ spectrometry measurements, including those made in 30 cm-deep probe holes when the radioactivity of the external structure is significantly different from the radioactivity of the measured block. For example, when the radioactivity of the front wall is twice that of the sediment block, the normalised γ Ḋ simulated for a 30 cm-deep probe hole is 8% higher than the normalised γ Ḋ simulated for an equivalent closed site with an inert wall. These configurations would be analogous to *in situ* γ spectrometry measurements made within granitic caves or rock shelters versus limestone caves or rock shelters.

4. Discussion

4.1. Representativeness of the simulations

Despite the many parameters taken into account in the models presented here, it is worth considering whether our simulations fully capture the complexity of real field measurement conditions; not only because of heterogeneity encountered at most sites, but also because the simulations require some simplifications of probe irradiation geometries. While acknowledging that the parameter configurations used in this study represent idealised scenarios primarily designed to quantify the relative influences of different parameters on *in situ* γ spectrometry assessments, the results obtained using the MIGAS code appear sufficiently suitable for reconstructing and correcting field γ Ḋ acquired in simple measurement configurations (at least in comparison to previously published datasets), such as those obtained in trenches dug within homogenous sediment, or situations where the probe measurement hole is < 30 cm.

Further refinement of the MIGAS code is also feasible, with planned changes including the possibility of undertaking site-specific simulations that implement more complex geometry configurations for the sediment or rock block and adjacent wall, and the ability to simulate stratified sediment deposits. However, simulations of more complex environments require significantly more empirical data than the basic configurations presented in this paper, including precise measurements of site geometry and independent characterisation of radioactivity conditions for different mineral strata and surrounding structures. The need to obtain detailed data prior to configuring site-specific MIGAS code may limit the usefulness of this approach in routine dating studies. In advance of the planned refinements to the MIGAS code, it is possible to undertake simulations of complex geometries and stratified sediment deposits using the DosiVox software (Martin et al., 2015a; Martin et al., 2015b; Martin et al., 2015c; Duval and Martin, 2019). However, in contrast to MIGAS, DosiVox cannot simulate γ spectrometry measurements and the threshold approach. This is one of the reasons why MIGAS was originally developed, as it offers the ability to determine γ Ḋ relationships and contributions for different points in the simulated environment.

The results shown in Fig. 10 highlight minor deviations in the MIGAS modelling output that may reflect simplifications of the probe irradiation geometry. In particular, for the configuration involving a front wall having radioactivity equivalent to the block, it is noticeable that the normalised γ Ḋ values are slightly below 100% for probe measurement depths of 0–35 cm (97.5–99.0%) compared to the γ Ḋ from simulated measurements in infinite matrix conditions (4π). This slight underestimation of the infinite matrix γ Ḋ does not seem to reflect γ absorption in the intervening air space, as the offset remains consistent if the distance between the wall and the block is varied (data not shown). Small variations with probe depth can also be observed for this dataset (blue curve in Fig. 10), particularly for simulated measurement depths of 5 cm–10 cm. These variations are not simply caused by statistical uncertainty as the same trends are apparent when undertaking repeated simulations or when increasing the number of particles simulated in a given run. Interestingly, the normalised γ Ḋ offsets and variations disappear if the simulated probe and measurement hole are replaced by sediment grains having the same radioactivity as the sediment block. In this case, the simulated γ Ḋ at any given depth equates to 100% of the infinite matrix γ Ḋ simulated at 80 cm depth. Though we cannot yet discount the possibility of minor artefacts in the γ probe simulation processes, it is possible that these effects are caused by local γ Ḋ distortions due to the presence of the inert probe itself. In most models, the probe is assumed to have a negligible effect on the γ Ḋ at the point of measurement (Lovborg and

Kirkegaard, 1974). However, the size and mass of the probe is non-negligible with respect to environmental γ particles, and it is therefore possible that this previous assumption is not upheld properly. Further investigations using different simulated probe sizes will be carried out to investigate this possible explanation. Irrespective, the effects on simulated or measured γ spectrometer Ḋ are small, and likely negligible for routine dating or modelling scenarios.

All simulations in this study have been carried out using a 2 × 2 inch NaI crystal probe, which is the most commonly used scintillator for luminescence and ESR dating applications. While it is likely that additional simulations carried out with probes of different sizes may yield slightly different results, the overall trends and magnitudes of effects should remain similar to those presented here. However, if quantitative results are required for the correction of empirical datasets obtained using different sized probes, we recommend carrying out tailored simulations using the MIGAS code and modifying the block hole and probe conditions accordingly.

As noted earlier, our simulations have not explicitly considered variations in detector efficiency with energy deposited in the crystal, or variations in photon transmission within the crystal. These parameters may vary significantly from one detector to another, and taking their full possible ranges into account is presently not feasible. Furthermore, similar to the probe size considerations indicated above, it is unlikely that these probe-specific efficiency or transmission properties would induce major changes in the trends or magnitudes of the effects observed in this study.

4.2. Quantifying the impact on γ Ḋ determination

Figs. 6 and 8 show that differences in material density and water content change the γ Ḋ resulting from simulated measurements by only a few percent. The magnitude of these changes is within the typical uncertainty ranges of field γ Ḋ measurements and therefore may be considered insignificant with regard to the final age uncertainty. It is also possible that these two effects may partially compensate each other for low-density sediment material, as these types of deposits are often characterized by high porosity, which favours high water content conditions. However, it is always better to take these effects into account, where possible, to improve the accuracy of dosimetric dating results. Knowing how these parameters influence the resulting γ Ḋ reduces the risk of bias, particularly where spectrometers have been calibrated using materials that are significantly different from naturally occurring sediments encountered in luminescence and ESR dating studies (e.g., calibrations performed using dense granitic rock slabs versus field measurements made in low-density organic soils). The data provided in this study (see Supplementary Material for full numerical datasets), as well as the MIGAS modelling codes used in our simulations, make this possible.

The depth and shape of probe holes used for field γ spectrometry have more significant combined effects on the resultant simulated γ Ḋ (Figs. 4 and 5). If these complicating effects are not properly considered, the resulting γ Ḋ may be biased by $>10\%$, with significant repercussions for dating accuracy. Similarly, external γ Ḋ contributions from surrounding structures can influence *in situ* γ Ḋ evaluations made in closed environments such as caves, rock shelters or trenches (Fig. 10). External γ Ḋ contributions can act to simplify *in situ* γ Ḋ evaluations if the radioactivity of the external environment is similar to that of the sediment blocks radioactivity, since the γ spectrometry Ḋ will be independent of hole depth and presumably hole shape. However, if the measured sediment block and its surrounding environment have significantly different radioactivities, the resultant *in situ* γ Ḋ evaluations can be inaccurate by ~5% for measurements made in 30 cm-deep holes or inaccurate by over 50% for measurements made in shallow holes (<5 cm depths) or at the sediment surface (0 cm depth).

Our simulations also confirm that field γ spectrometry measurements carried out in 2π geometry yield less than 50% of the infinite matrix γ Ḋ for open field sites. This is due to a deficit of backscattered γ particles on the surface of the sediment or rock block. In contrast, simulations of 2π geometry field γ spectrometry measurements made at (semi-)closed sites equate to 50% of the infinite matrix γ Ḋ due to backscattering of γ particles on nearby inert structures. From a practical perspective, it is worth noting that for most open-air scenarios it is very unlikely that γ Ḋ measured in 2π geometry would be significantly less than half the infinite matrix γ Ḋ owing to backscattered γ contributions from all structures in the surrounding area (those within the γ range for air), as well as external contributions from cosmic radiations (Lovborg and Kirkegaard, 1974), although the latter is usually removed by considering an upper threshold at 2800 keV. Nevertheless, the relative differences in backscattered/external γ Ḋ contributions between open field and closed sites is significant, and particularly relevant for γ spectrometry measurements made using shallow probe holes when the surrounding radioactive environments are different from those prevailing during original calibration of the scintillator probe.

4.3. Mitigating against biases related to field measurement conditions

One of the main objectives of this study was to examine practical methods for mitigating against biases induced by field γ spectrometry measurements made under conditions that differ from those of the original spectrometer calibration. Our first advice is not new but more a reminder of good practice: it is necessary to know the conditions at the time of calibration, and the methods used to derive the reference values for the calibration material. For example, the Oxford calibration blocks, which are the most widely used in the luminescence and ESR dating community, were originally calibrated using CaF_2 dosimeters, which compensates for a slight potential bias on the Th γ emissions that might result from the relatively-limited size of the blocks (Rhodes and Schwenninger, 2007). The calibration block Ḋ values deduced from these dosimeters assume infinite matrix conditions. As such, calibration of a γ spectrometer using the Oxford blocks implies that 4π geometry is considered, i.e., the spectrometer is calibrated to give the exact Ḋ recorded at the point of measurement. Therefore, when calibrated in this way, a spectrometer probe inserted in a 30 cm-deep hole at a given study site will only give 95% of the infinite matrix Ḋ in the absence of external contributions (Fig. 4). This could equate to a 5% systematic underestimation of the γ Ḋ measured at a given site if not duly considered (e.g., by applying a correcting factor). To avoid such bias, it is important to be aware of the assumptions behind, and approaches used to derive, the reference values of calibration materials and, if possible, to mimic expected field conditions as close as possible when calibrating the spectrometer probe.

When field conditions preclude digging a hole deep enough to ensure infinite matrix conditions are upheld, it is possible to extract depth correction factors from the data provided in Fig. 4 (see Supplementary Material SD1 for numerical data), provided that the depth of the measurement hole is recorded in the field. Similarly, the data shown in Fig. 5 can be used to estimate correction factors as a function of measurement hole shape in the field (see Supplementary Material SD2). Though our simulations do not cover a wide range of hole shapes and sizes, we plan to undertake further simulations to derive a more tailored range of correction factors in the future. It is worth keeping in mind, however, that it can be difficult to determine the exact shape of the probe hole in the field. The optimal solution therefore remains keeping the size and shape of the hole as close as possible to that of the probe itself.

Several options are available for mitigating against the limited impacts of material density, composition and water content effects on measured γ Dr. Calibrating the spectrometer in various materials and under different water content regimes would represent the ideal solution. However, this is probably the least convenient and most complicated approach, as it would require building (or accessing) new certified calibration structures. An alternative (easier) solution would be to characterise the material (i.e., nature, approximate density and water

content) and use the data from our simulations to derive correction factors (see Supplementary Material SD3 and SD4). Finally, an additional systematic uncertainty could also be included on the γ Ḋ value to account for variability in material density and composition (i.e. an additional uncertainty of up to 4% on the γ Dr), as well as for the water attenuation factor error (an additional 1%–4% depending on the water content of the sediment, see SD5).

In all cases, it is crucial to take into account differences in the χ value calculated for the spectrometer probe and the χ value published previously for sediment grains when making γ Ḋ measurements in wet sediments (e.g. deposits approaching saturated water conditions, including sediments encountered in caves or beach environments). γ Ḋ measured using scintillator probes are effectively water corrected at the time of acquisition according to χ values that are relevant for centimetric-sized objects (such as the value of 1.02 ± 0.03 derived in our simulations). However, such χ values differ from those of relevance for dating smaller objects such as sediment grains (1.14 ± 0.03). Corrections are therefore needed to account for these issues when undertaking luminescence and ESR age calculations. Two scenarios, in particular, are worth considering for correcting age calculations: (i) *in situ* γ Ḋ measurement made in wet sediment, where the present-day water content is considered representative of that prevailing during the burial period (though this assumption may not always be robust; e.g. Liritzis and Galloway, 1981); and (ii) *in situ* γ Ḋ measurements made in wet sediment, where the present-day water contents are not representative of those prevailing during the entire burial period. In the latter case, it is necessary to first calculate a dry γ Ḋ for the scintillator probe and then calculate a relevant wet γ Ḋ for the dated sediment grains using the best estimate of the average water content over the burial period. For scenario (i), there would be an overestimation of the calculated γ Ḋ for sediment grains when directly using the γ Ḋ value measured by portable γ spectrometry, as shown in Fig. 8. For scenario (ii), there would also be an overestimation of the dry γ Ḋ if the conversion is made using the standard χ value for sediment grains (1.14 ± 0.03). This would subsequently lead to an overestimation of the long-term wet γ Ḋ recalculated from the dry γ Ḋ data. In both cases, a more accurate way of determining the sediment grain γ Ḋ from γ spectrometry measurements performed in wet condition would be to first calculate a dry γ Ḋ using the χ value relevant for the spectrometer probe (1.02 ± 0.03). From this dry γ Dr, it is then possible to recalculate the wet γ Ḋ for sediment grains using the χ value of 1.14 ± 0.03, together with the best estimate of the average water content over the burial period (either the present-day water content or an assumed water content that differs from the present-day conditions).

Typically, there is significant inter-site variability in external γ Ḋ contributions from surrounding structures, which makes it difficult to apply simple correction factors deduced from tabulated data (e.g., those shown in Supplementary Material SD6 and SD7). Moreover, the geometry of the surrounding environment at any given site is usually more complex than the scenarios modelled in this study. Guérin and Mercier (2011b) proposed that external γ Ḋ contributions could be determined by performing γ Ḋ measurements in 2π geometry with and without an attenuation layer being placed in front of the sediment surface. If the γ attenuation properties of the intervening material is known, and the layer only attenuates γ emissions originating from the sediment block, then the γ Ḋ determined with and without the attenuation layer can be used to isolate the γ Ḋ contribution from the sediment block itself. The sediment γ Ḋ contribution is then assumed to represent 50% of the infinite matrix γ Ḋ in 4π geometry. While this method should work in open environments, it could lead to underestimation of the external γ Ḋ contributions in (semi-)closed environment because of potentially significant backscattered γ Ḋ contributions to the sediment surface. An additional correction should therefore be included to account for such backscattered γ Ḋ contributions in closed environments. An alternative solution could be to carry out repeated *in situ* γ spectrometry measurements at increasing probe depths, in order to separate the external γ Ḋ contributions from the γ Ḋ originating from the sediment or rock of interest. One could for example measure the γ Ḋ at the surface (i.e., in 2π geometry) and then 20 cm deeper at the same location, and then use the difference in measured γ Ḋ to quantify external γ contributions (Fig. 10) and remove them from the measured γ Ḋ. Of course, it is possible to perform multiple measurements at various depths to increase the accuracy of such analysis, but this would be at the cost of increased measurement time. Unfortunately, this solution may not be practical at sensitive archaeological sites where the creation of measurement holes could compromise conservation of the site. In such circumstances, it may only be possible to perform surface measurements, and external γ Ḋ contributions from the surrounding environment must then be evaluated differently; either following Guérin and Mercier (2011b) but with the inclusion of a calibration for backscattered γ components (as detailed above), or by undertaking full γ Ḋ modelling of the site (e.g., Hood and Highcock, 2019).

Irrespective of all these considerations, it should be borne in mind that the suitability of field γ spectrometry measurements for dosimetric dating studies is always dependent on a series of approximations, or assumptions, including: (i) the sedimentary section used for *in situ* γ Ḋ evaluation has the same properties as the broader sedimentary deposit under consideration for dating, (ii) the Ḋ has not significantly changed other time, and (iii) the γ Ḋ at the point of measurement is representative of the γ Ḋ absorbed by the dated sample. The validity of these assumptions needs to be carefully evaluated on a site-by-site basis to guarantee the reliability of *in situ* γ Ḋ determination. Reconstructing the environment before excavation and modelling the γ Ḋ can be a useful tool for interrogating these assumptions (Hood and Highcock, 2019). It is likely that Monte Carlo modelling approaches will be increasingly employed in the near future with the development of 3D imaging methods. For this purpose, the Geant4 MIGAS code is particularly useful and is available on request from the authors.

5. Conclusion

Field γ Ḋ measurement conditions can vary significantly from the ideal conditions that exist at the time of instrument calibration owing to heterogeneity in material composition, water content, matrix compaction, and surrounding environments encountered in natural open air and closed sites. In this context, Monte Carlo modelling offers a unique opportunity to investigate and quantify the impacts of several parameters of relevance for portable γ spectrometer Ḋ determination (e.g., depth and size/shape of the probe measurement hole; the nature, density and water content of the sediment or rock measured; the presence of external structures such as walls). Knowing the extent to which these parameters can bias *in situ* γ Ḋ evaluations provides a means to develop mitigating solutions.

Our simulations reveal that variability in material composition, density and water contents typically have small, but not necessarily negligible, effects on *in situ* γ Ḋ evaluations. Appropriate correction factors can be derived using the data presented in this study, and these should allow improvements in the accuracy of γ Ḋ measurements performed at typical sites. The shape and depth of the measurement hole can have significant impacts on the reliability of γ spectrometry measurements, as well as the extent to which external γ contributions will influence the calculated Ḋ. While corrections using the data presented here are possible, they necessitate careful assessment of the geometry and dimensions of measurement holes on an individual basis. This is why we strongly recommend to precisely record the in situ gamma dose rate measurement conditions while in the field. External and backscattered contributions to γ Ḋ measurements could be constrained by performing *in situ* measurement at different depths. Once quantified, these external contributions can be subtracted from γ Ḋ measurements made in 2π geometry if necessary.

Although γ Ḋ modelling is a powerful tool for testing multiple hypotheses, its use for deriving corrections for specific sites or individual γ spectrometry measurements remains limited. As noted above, field

conditions are often considerably more complex and varied than the scenarios considered in this study, and the creation of refined models tailored to individual sites or measurements would require considerable amounts of time, data and resources.

In light of the promising results obtained in this study, more simulations with the MIGAS code are planned to expand the existing datasets and further investigate the effect of a broader range of parameters on field γ spectrometry (e.g., different probe sizes and compositions). We also plan to undertake complementary experimental γ spectrometry measurements under controlled conditions in order to validate our existing, and future modelling results.

Declaration of competing interest

The authors declare that they have no known competing financial interests or personal relationships that could have appeared to influence the work reported in this paper.

Data availability

the results data are provided in Supporting File, all other data including spectra and codes will be made available on request

Acknowledgements

The Spanish Ramón y Cajal Fellowship RYC 2018-025221-I granted to MD is funded by MCIN/AEI/10.13039/501100011033 and by 'ESF Investing in your future'. This work is part of Grant PID 2021-123092NB-C22 funded by MCIN/AEI/10.13039/501100011033/'ERDF A way of making Europe'.

Appendix A. Supplementary data

Supplementary data to this article can be found online at https://doi.org/10.1016/j.radphyschem.2023.111365.

References

Agostinelli, S., Allison, J., Amako, K., Apostolakis, J., Araujo, H., Arce, P., Asai, M., Axen, D., Banerjee, S., Barrand, G., Behner, F., Bellagamba, L., Boudreau, J., Broglia, L., Brunengo, A., Burkhardt, H., Chauvie, S., Chuma, J., Chytracek, R., Cooperman, G., Cosmo, G., Degtyarenko, P., Dell'Acqua, A., Depaola, G., Dietrich, D., Enami, R., Feliciello, A., Ferguson, C., Fesefeldt, H., Folger, G., Foppiano, F., Forti, A., Garelli, S., Giani, S., Giannitrapani, R., Gibin, D., Cadenas, J. J. Gomez, Gonzlez, I., Abril, G. Gracia, Greeniaus, G., Greiner, W., Grichine, V., Grossheim, A., Guatelli, S., Gumplinger, P., Hamatsu, R., Hashimoto, K., Hasui, H., Heikkinen, A., Howard, A., Ivanchenko, V., Johnson, A., Jones, F.W., Kallenbach, J., Kanaya, N., Kawabata, M., Kawabata, Y., Kawaguti, M., Kelner, S., Kent, P., Kimura, A., Kodama, T., Kokoulin, R., Kossov, M., Kurashige, H., Lamanna, E., Lampen, T., Lara, V., Lefebure, V., Lei, F., Liendl, M., Lockman, W., Longo, F., Magni, S., Maire, M., Medernach, E., Minamimoto, K., de Freitas, P. Mora, Morita, Y., Murakami, K., Nagamatu, M., Nartallo, R., Nieminen, P., Nishimura, T., Ohtsubo, K., Okamura, M., O'Neale, S., Oohata, Y., Paech, K., Perl, J., Pfeiffer, A., Pia, M.G., Ranjard, F., Rybin, A., Sadilov, S., Salvo, E. Di, Santin, G., Sasaki, T., Savvas, N., Sawada, Y., Scherer, S., Sei, S., Sirotenko, V., Smith, D., Starkov, N., Stoecker, H., Sulkimo, J., Takahata, M., Tanaka, S., Tcherniaev, E., Tehrani, E. Safai, Tropeano, M., Truscott, P., Uno, H., Urban, L., Urban, P., Verderi, M., Walkden, A., Wander, W., Weber, H., Wellisch, J.P., Wenaus, T., Williams, D.C., Wright, D., Yamada, T., Yoshida, H., Zschiesche, D., 2003. Geant4–a simulation toolkit. Nucl. Instrum. Methods Phys. Res. Sect. A Accel. Spectrom. Detect. Assoc. Equip. 506 (3), 250–303.

Aitken, M.J., 1985. Thermoluminescence Dating. Academic Press, London, p. 378.

Aitken, M.J., Xie, J., 1990. Moisture correction for annual gamma dose. Ancient TL 8, 6–9.

Arnold, L.J., Duval, M., Falguères, C., Bahain, J.-J., Demuro, M., 2012. Portable gamma spectrometry with cerium-doped lanthanum bromide scintillators: Suitability assessments for luminescence and electron spin resonance dating applications. Radiat. Meas. 47, 6–18.

Baró, J., Sempau, J., Fernández-Varea, J.M., Salvat, M., 1995. PENELOPE: an algorithm for Monte Carlo simulation of the penetration and energy loss of electrons and positrons in matter. Nucl. Instrum. Methods Phys. Res. B 100, 31–46.

Duval, M., Arnold, L.J., 2013. Field gamma dose-rate assessment in natural sedimentary contexts using LaBr3(Ce) and NaI(Tl) probes: a comparison between the "threshold" and "windows" techniques. Appl. Radiat. Isot. 74, 36–45. https://doi.org/10.1016/j.apradiso.2012.12.006.

Fain, J., Soumana, S., Montret, M., Miallier, D., Pilleyre, T., Sanzelle, S., 1999. Luminescence and ESR dating Beta-dose attenuation for various grain shapes calculated by Monte-Carlo method. Quat. Geochronol. 18, 231–234.

Guérin, G., Mercier, N., 2011a. Determining gamma dose rates by field gamma spectroscopy in sedimentary media: results of Monte Carlo simulations. Radiat. Meas. 46, 190–195. https://doi.org/10.1016/j.radmeas.2010.10.003.

Guérin, G., Mercier, N., 2011b. Field gamma spectrometry, Monte Carlo simulations and potential of non-invasive measurements". Geochronometria 39, 40–47. https://doi.org/10.2478/s13386-011-0056-z.

Guérin, G., Mercier, N., 2012. Preliminary insight into dose deposition processes in sedimentary media on a scale of single grains: Monte Carlo modeling of the effect of water on the gamma dose rate. Radiat. Meas. 47 (issue 7), 541–547.

Hauf, S., Kuster, M., Batič, M., Bell, Z.W., Hoffmann, D.H.H., Lang, P.M., Neff, S., Pia, M. G., Weidenspointner, G., Zoglauer, A., 2013. Radioactive decays in Geant4. IEEE Trans. Nucl. Sci. 60, 2966–2983. https://doi.org/10.1109/TNS.2013.2270894.

Hood, A., Highcock E., 2019. Using to Reconstruct Radiation Transport through Complex Archaeological Environments. Methods and protocols. 2. 10.3390/mps2040091.

Ivanchenko, V., Apostolakis, J., Bagulya, A., Abdelouahed, H.B., Black, R., Bogdanov, A., Burkhard, H., Chauvie, S., Cirrone, P., Cuttone, G., Depaola, G., Di Rosa, F., Elles, S., Francis, Z., Grichine, V., Gumplinger, P., Gueye, P., Incerti, S., Ivanchenko, A., Jacquemier, J., Lechner, A., Longo, F., Kadr, O., Karakatsanis, N., Karamitros, M., Kokoulin, R., Kurashige, H., Maire, M., Mantero, A., Mascialino, B., Moscicki, J., Pandola, L., Perl, J., Petrovic, I., Ristic-Fira, A., Romano, F., Russo, G., Santin, G., Schaelicke, A., Toshito, T., Tran, H., Urban, L., Yamashit, T., Zacharatou, C., 2011. Recent improvements in Geant4 electromagnetic physics models and interfaces. Progr.Nuclear. Sci. Technol. 2, 898–903.

Koivunoro, H., Siiskonen, T., Kotiluoto, P., Auterinen, I., Hippelainen, E., Savolainen, S., 2012. Accuracy of the electron transport in mcnp5 and its suitability for ionization chamber response simulations: a comparison with the EGSNRC and PENELOPE codes. Med. Phys. 39, 1335–1344. https://doi.org/10.1118/1.3685446.

Liritzis, Y., Galloway, R.B., 1981. Correlation of variation in the γ-ray dose-rate in soil with meteorological factors. Archaeometry 23, 109–113.

Liritzis, Y., 1989. Dating of Calcites: some aspects of radiation survey in caves and dose-rates. Annales géologiques des pays helléniques 34, 123–136.

Lovborg, L., Kirkegaard, P., 1974. Response of 3″× 3″NaI(Tl) detectors to terrestrial gamma radiation. Nucl. Instrum. Methods 121, 239–251. https://doi.org/10.1016/0029-554X(74)90072-X.

Løvborg, L., Bøtter-Jensen, L., Kirkegaard, P., Christiansen, E.M., 1979. Monitoring of soil natural radioactivity with portable gamma-ray spectrometer. Nucl. Instrum. Methods 167, 341–348. https://doi.org/10.1016/0029-554X(79)90021-1.

Martin, L., Incerti, S., Mercier, N., 2015c. Comparison of DosiVox simulation results with tabulated data and standard calculations. Ancient TL 33 n°2, 1–9.

Martin, L., Mercier, N., Incerti, S., Lefrais, Y., Pecheyran, C., Guerin, G., Jarry, M., Bruxelles, L., Bon, F., Pallier, C., 2015b. Dosimetric study of sediments at the beta dose rate scale: characterization and modelization with the DosiVox software. Radiat. Meas. 81 SI, 134–141. https://doi.org/10.1016/j.radmeas.2015.02.008.

Martin, L., Incerti, S., Mercier, N., 2015a. DosiVox: implementing Geant 4-based software for dosimetry simulations relevant to luminescence and ESR dating techniques. Ancient TL 33–1, 1–10.

Mercier, N., Falguères, C., 2007. Field gamma dose-rate measurement with a NaI(Tl) detector: re-evaluation of the "threshold" technique. Ancient TL 25, 1–4.

Murray, A.S., Bowman, S.G.E., Aitken, M.J., 1978. Evaluation of the gamma dose-rate contribution. PACT 2, 84–96.

Nathan, R.P., Thomas, P.J., Jain, M., Murray, A.S., Rhodes, E.J., 2003. Environmental dose rate heterogeneity of beta radiation and its implications for luminescence dating: Monte Carlo modeling and experimental validation. Radiat. Meas. 37, 305–313.

Nathan, R.P., Mauz, B., 2008. On the dose-rate estimate of carbonate-rich sediments for trapped charge dating. Radiat. Meas. 43 (1). January.

Rhodes, E.J., Schwenninger, J.-L., 2007. Dose rates and radioisotope concentrations in the concrete calibration blocks at Oxford. Ancient TL 25 (1), 5–8.

Saito, K., Moriuchi, S., 1981. Monte Carlo calculation of accurate response functions for a NaI(Tl) detector for gamma rays. Nucl. Instrum. Methods Phys. Res. 185, 299–308. https://doi.org/10.1016/0029-554X(81)91225-8.

Zimmerman, D.W., 1971. Thermoluminescent dating using fine grains from pottery. Archaeometry 10, 26–28.